16.3   Embedded cellular convection in moist flow past two-dimensional topography

Oliver Fuhrer[1]* and Christoph Schär[1]

[1] Institute for Atmospheric and Climate Science, ETH Zürich, Switzerland

1. Introduction

In order to explain the high precipitation amounts and efficiencies frequently observed in orographic precipitation events Smith (1979) proposed the presence of shallow embedded convection in nominally stratiform events. The convective updrafts increase the amount of lifting and subsequent condensation individual air parcels experience. In these pockets of enhanced cloud water content, the microphyiscal processes (i.e. conversion of cloud water to rain water and collection of cloud water by rainwater) are intensified. Thus, the presence of cellular convection within an orographic cloud may substantially enhance the precipitation amount, precipitation effciency, and rainfall intensity. In this study, the development, structure and impact of embedded cellular convection in orographic clouds is addressed.

A necessary but not sufficient ingredient for the development of embedded convection are regions of statically unstable stratification. These regions can be diagnosed by a negative sign of N_m^2, where N_m is the moist Brunt-Väsäilä frequency (Emanuel 1994). While the presence of statically unstable regions is a necessary condition for buoyant instabilities to grow, many other factors govern the onset and structure of embedded convection (Kirshbaum and Durran 2004). In the present work, three of these environmental factors are addressed: random heterogeneities in the impinging air-mass, upstream profile stability and the presence of small-scale topographic features.

2. Experimental Design

A mesoscale model, Advanced Regional Prediction System (ARPS, Xue et al. 2000) is used for this study. ARPS is a fully non-hydrostatic cloud resolving model using a terrain-following coordinate system. The

subgrid-scale turbulence closure is a first-order scheme based on Lilly (1962), and warm-rain microphysics are included using a Kessler parametrization. Other physical parametrizations are not included for the sake of simplicity.

The model setup can be described as follows. The computational domain spans 500 km in the inflow direction and is 50 km wide. A horizontal resolution of 500 m is used for all simulations. An isolated bell-shaped ridge is located at $x = 300\,km$ and is defined by the following equation

$$h(x) = h_0 \frac{a^2}{a^2 + x^2}, \qquad (1)$$

where $h_0 = 1\,km$ is the height of the ridge and $a = 20\,km$ is the ridge half width. The flow field is initialized using a pseudo-sounding derived analytically from the follwing parameters: a constant surface air temperture T_s, a constant dry buoyancy frequency $N_d = 0.011\,s^{-1}$, a uniform wind $U = 15\,ms^{-1}$ and a constant relative humidity $RH = 95\%$. In order to break the y-symmetry of the initial flow field and seed convective elements random perturbations are introduced into the potential temperature field. The perturbations are filtered three times removing completely $2\Delta x$-waves and are shifted and rescaled to have a mean value of zero and a fixed maximum norm $|\delta\theta|_\infty$.

Figure 1a shows the idealized soundings corresponding to experiments T280 through T292.5 in 2.5 K intervals, where the name of the experiments corresponds to the surface temperature T_s. The corresponding profiles of θ_e are shown in **Figure 1b**. Already the coldest T280 profile exhibits marginal potential instability (PI) from the surface up to about 500 m. With increasing profile temperature and implied specific humidity, the strength and layer thickness of the PI increases. T292.5 exhibits a strongly potentially unstable layer of approximately 5 km thickness. Using this set of idealised upstream profiles we can systematically investigate the effect of increasing upstream conditional and potential instability on cloud formation and precipitation for flow over a mountain ridge. Differences in the sim-

*Corresponding author: Oliver Fuhrer, Institute for Atmospheric and Climate Science ETH, Winterthurerstrasse 190, 8057 Zürich, Switzerland. Email: oliver.fuhrer@env.ethz.ch
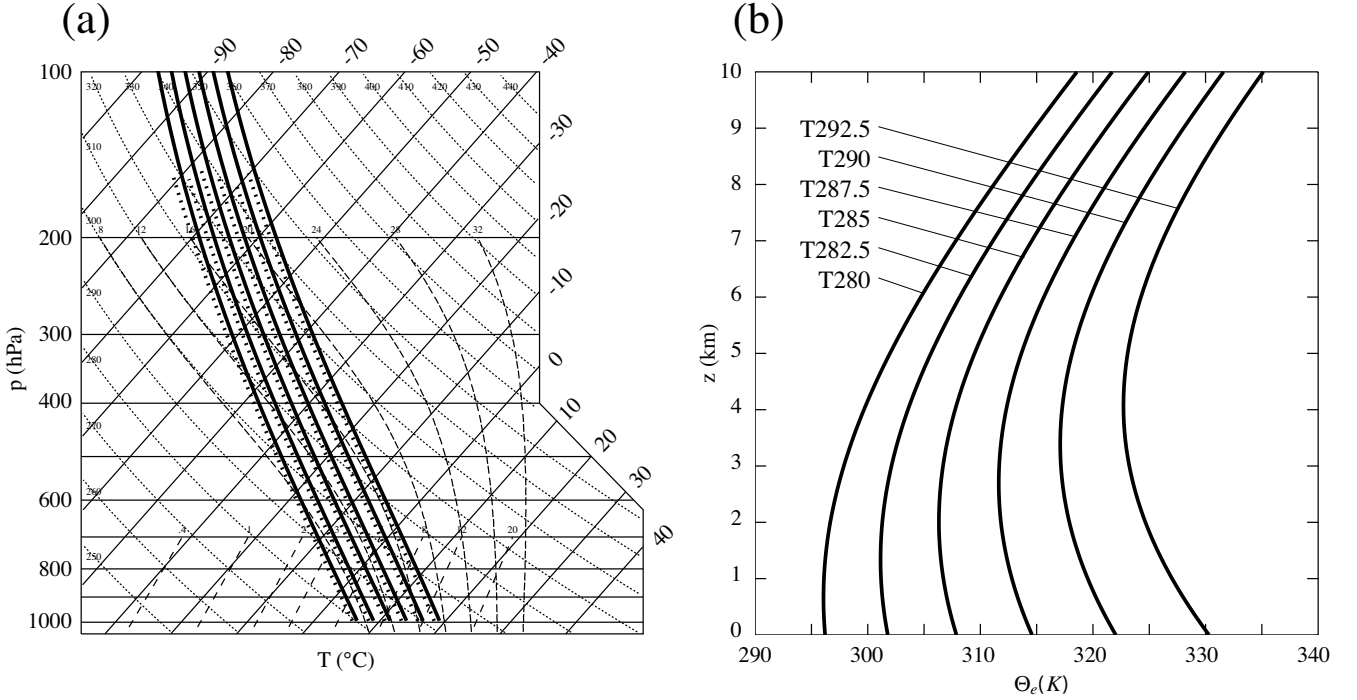
Figure 1: Idealized (a) p-skew-T profiles and (b) θ_e profiles for increasing overall profile temperature. Shown are T280, T282.5, T285, T287.5, T290, T292.5 and T295 corresponding to the curves left to right respectively in both panels.

ulations' flow dynamics can be attributed to the effects of latent heating and microphysics feedback on the dynamics.

3. Results

a. *Towards Embedded Cellular Convection*

Results from the coolest simulation T280 are shown in **Figure 2a**. The moist low-level air rises stably over the ridge and a quasi-stationary stratiform cap cloud develops directly over the ridge peak. The impinging airmasses easily surmount the topographic obstacle and no upstream blocking or flow reversal occurs. The simulation preserves the along-ridge translational symmetry of the experimental setup over the whole integration period.

The cloud water field for the next warmer simulation (T285) depicted in **Figure 2c**, give an indication of cellular perturbations within the orographic cloud. The strongest perturbations are located close to the cloud border in the lee of the ridge. However, the perturbations do not grow to fully developed convective cells. Perturbations in the vertical wind are on the order of 5 cm/s corresponding to 5% of the vertical velocities due

to forced ascent over the ridge. Even though a 1 km deep region of unstable stratification ($N_m^2 < 0$) within the cap cloud is present, the growth rate of the buoyant instabilities is comparable to the advective timescale and thus, the buoyant instabilities do not have sufficient time to grow into convective updrafts.

Experiment T290 (see **Figure 2e**) shows a different flow regime. Horizontal cross-sections of q_c (**Fig. 2c,d**) show that wave-like perturbation on the upslope of the ridge quickly grow into fully developed convective updrafts well before the ridge top. The cloud pattern is clearly reminiscent of the open-cell circulations of mesoscale cellular convection (MCC), which is observed frequently in boundary layer convection for example during cold air outflows over the ocean (see Atkinson and Zhang (1996) for a review article). The open-cell type of convection is characterised by honeycomb shaped cells with downward motion and clear sky in the cell center, surrounded by cloud associeted with upward motion. The cell diameter can be estimated to around $9 - 12 \, km$. Maximum updraft velocities are 8 m/s and 12 m/s, respectively. Timeseries of $|q_c|_{max}$ indicate that the convective updrafts contain pockets of increased cloud liquid water contents which are a factor of 2.1 larger than what could be achieved by simple forced stable ascent over the ridge. Updrafts are clearly
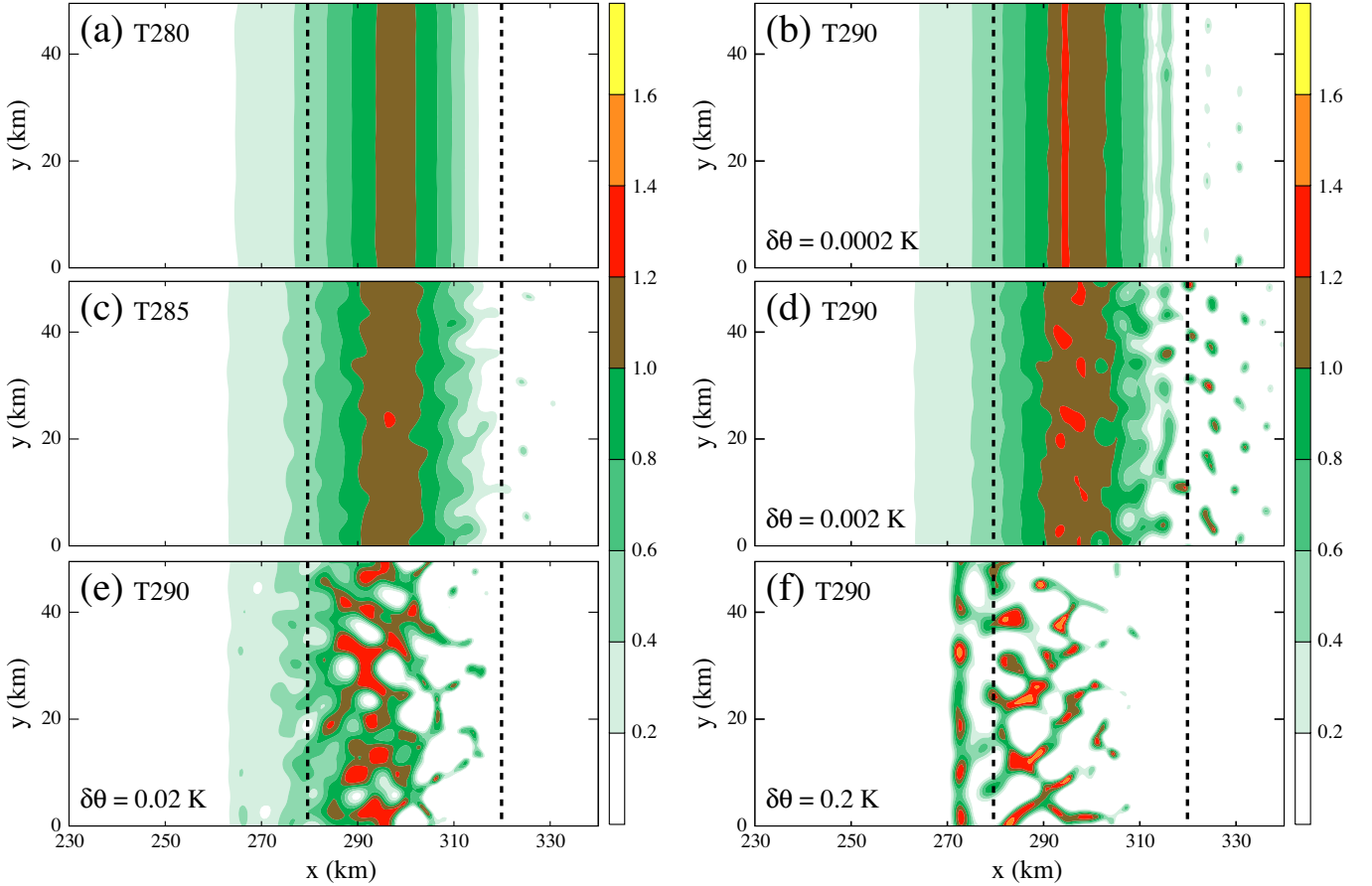
Figure 2: Left: comparison of simulations of increasing surface temperature T_s, namely (a) T280, (c) T285 and (e) T290 at $t = 5\,h$. Shaded contours show q_c in g/kg at $z = 1.5\,km$. Half height of topography is indicated by thick dashed lines. Right: comparison of simulations with increasing perturbation amplitude, namely (b) $\delta\theta = 0.0002\,K$, (d) $\delta\theta = 0.002\,K$ and (f) $\delta\theta = 0.2\,K$. Note that the simulation with $\delta\theta = 0.02\,K$ is shown in panel (e).

collocated with high q_c and surrounded by cloud free regions associated with compensating subsidence.

The domain averaged rain rates R_{steady} in quasi-steady state and maximum observed rain rates R_{max} are listed in **Table 1**. The maximum rain rate of 0.63 mm/h is typical for light rain. For the T280 experiment precipitation is soley due to the forced ascent over the topographic barrier. Since no blocking or flow around occurrs for our particular experimental setup, maximum cloud liquid water concentrations are found close to the ridge peak. This maximum is collocated with a maximum in production of precipitable water (not shown).

R_{steady} and R_{max} increase slowly with increasing upstream profile temperature (cf. **Tab. 1**) from T280 to T287.5. This increase is consistent with the respective increase of total column water. The precipitation measures of T290 and T292.5 are drastically increased due to the convective dynamics. Maximum instanta-neous rain rates peak at $105\,mm/h$ and $185\,mm/h$ for the two cases, respectively. This jump can only be explained by a more efficient depletion of the available water vapour due to the embedded cellular convection. There are some choices regarding its computation and we look at two measures. The first, PE_{dyn} is defined by the ratio of instantaneous precipitation to the condensation rate. Evaporation of condensed water is not accounted for. This efficiency measure takes into account the flow dynamics, since the dynamics directly determines the amount of condensation. The second, PE_{bulk} is motivated by a box argument. It is defined by the ratio of total precipitation in a control volume to the total water vapour which enters the control volume. In our case we consider the whole domain as our control volume. Values of PE_{dyn} and PE_{bulk} are listed in **Table 1**. Both measures show a jump in efficiency from T287.5 to T290. The increase is somewhat less pronounced for PE_{bulk} since only a fraction of the incoming water

3

Table 1: Various precipitation measures for increasing upstream potential instability: domain averaged rain rate R_{steady}, maximum rain rate R_{max}, percentage of condensed water which reaches the ground PE_{dyn}, percentage of inflow moisture which reaches the ground. All quantities are evaluated for the interval $4\,h < t < 5\,h$.

T_s (K)	R_{steady} $(10^6 kg/s)$	R_{max} (mm/h)	PE_{dyn} $(\%)$	PE_{bulk} $(\%)$
280	0.11	0.63	2.9	1.0
282.5	0.18	0.99	4.1	1.3
285	0.25	1.5	5.3	1.5
287.5	0.34	3.0	6.2	1.7
290	1.1	105	15	6.5
292.5	2.3	185	16	7.8

vapour is actually processed by the orographic cloud.

b. *Stability of the flow solution*

The precedent results have all been performed with random perturbations introduced into the θ-field. We have chosen a maximum norm $|\delta\theta|_\infty = 0.02\,K$. In order to investigate the sensitivity of the flow solution to these perturbations, a series of experiments with $|\delta\theta|_\infty = 0.0002, 0.002, 0.02, 0.2\,K$ has been performed for the T290 upstream profile. Results are shown in **Figure 2b,d,e,f**, respectively. The cloud water field at $t = 5\,h$ indicate that convective cells grow soley due to the presence of finite amplitude perturbations in the upstream flow. If the perturbations are switched off the flow solution of all experiements collapse into a quasi-twodimensional solution very similar to **Figure 2b**. The location and speed of development of buoyant instabilities is clearly very sensitive to small-scale perturbations. For this particular flow setup, there is not upstream propagation of information from preexisting convective cells to trigger new instabilities. Further experiments (not shown) indicate that this may not be the case for smaller wind speeds and sheared wind profiles.

c. *Small-scale topographic disturbances*

Cosma et al. (2002) have performed simulations that suggest that small-scale orography may play a decisive role in forcing the location of precipitation in slightly potentially unstable flows. Their simulations indicate that precipitations bands are generated by horizontal convergence of the wind on the lee-side of small-scale topographic disturbances. Here we repeat the $T_s = 290\,K$ experiement but also introducing a small-scale topographic disturbance (STD) 80 km upstream of the ridge
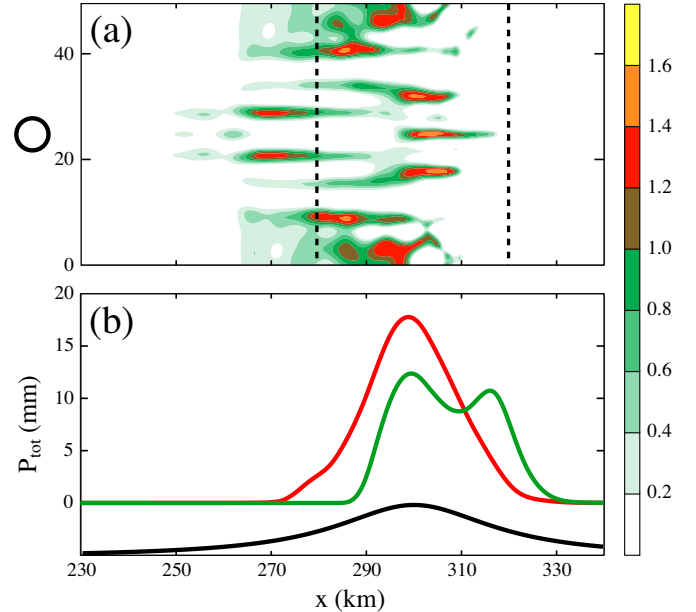
Figure 3: Upper panel: same figure as **Figure 2e** but with small-scale topographic disturbance. Lower panel: comparison of rainfall acumulation between reference simulation (green) and simulation with small-scale topographic disturbance (red).

top. The STD is of Gaussian shape with a height of 500 m and a half-width of 8 km. **Figure 3a** shows the cloud water content at $t = 5\,h$ and $z = 1.5\,km$. The location of the STD is indicated by a thick black isoline at its half height. The only difference compared to the simulation depicted in **Figure 2e** is the presence of the STD. Clearly, the STD has a strong impact: Convective updrafts in the lee of the small hill are organized in localized bands instead of a series of convective cells. A simulation without the ridge but just the STD (not shown) reveals that the triggering of the rain bands requires the presence of both the ridge and the STD. The far upstream location of the STD makes a direct dynamical influence unlikely. Irreversible vertical mixing due to convective overturning causes a permanent temperature and moisture anomaly in the lee of the STD. Consistent with the strong sensitivity to upstream perturbations shown above, this slight breaking of the y-symmetry of the airmass impinging on the ridge suffices to strongly modulate the development of convection. **Figure 3b** indicates that rainfall accumulation after five hours is shifted upstream and exhibits a larger amplitude directly above the ridge top. convection.

4

4. Conclusion

Results indicate that the presence of shallow embedded convection indeed considerably enhances the efficiency of condensate release in orographic precipitation. Also, maximum precipitation intensities and rainfall accumulation are substantially increased. It should be noted though, that in the cooler simulations the inclusion of ice-processes may also increase the precipitation efficiency.

Many factors influence the development and organization of shallow embedded convection in orographic precipitation. Here, three such factors have been addressed using an idelized modelling approach. The numerical results confirm, that upstream PI is not the only factor determining the development of embedded convection. If sufficient lifting occurrs it predicts well the presence of statically unstable regions, which are necessary for buoyant instabilities to exist. Evidence has been found that upstream perturbations (random or from small-scale topography) may strongly modulate the onset and structure of the convection.

References

Atkinson, B. W. and J. W. Zhang, 1996: Mesoscale shallow convection in the atmosphere. *Rev. of Geophyics*, **34**, 403–431.

Cosma, S., E. Richard, and F. Miniscloux, 2002: The role of small-scale orographic features in the spatial distribution of precipitation. *Q. J. R. Meteorol. Soc.*, **128**, 75–92.

Emanuel, K. A., 1994: *Atmospheric Convection*. Oxford University Press.

Kirshbaum, D. J. and D. R. Durran, 2004: Factors governing cellular convection in orographic precipitation. *J. Atmos. Sci.*, **61**, 682–698.

Lilly, D. K., 1962: On the numerical ismulation of buoyant convection. *Tellus*, **14**, 148–172.

Smith, R. B.: 1979, The influence of mountains on the atmosphere. *Adv. Geophysics*, volume 21, 87–230.

Xue, M., K. Droegemeier, and V. Wong, 2000: The Advanced Regional Prediction System (ARPS) - a multisclae nonhydrostatic atmospheric simulation and prediction model. part I: Model dynamics and verification. *Meteorol. Atmos. Phys.*, **75**, 161–193.